Kinetics of the Simultaneous Phase Separation and Gelation in Solutions of Dextran and Gelatin

R. H. Tromp,* A. R. Rennie, and R. A. L. Jones

Cavendish Laboratory, University of Cambridge, Madingley Road, Cambridge CB3 0HE, United Kingdom

Received November 15, 1994; Revised Manuscript Received March 13, 1995®

ABSTRACT: Influences of gelation on the kinetics of the phase separation in a mixed, aqueous solution of dextran and gelatin have been studied. The solution separates into dextran-rich and gelatin-rich phases below a phase transition temperature. For a deeper quench, the solution gels as well as phase separates. Results of time-resolved small-angle elastic light scattering and phase contrast microscopy for quenches near the critical point show that above the gelation temperature phase separation is followed by spinodal decomposition and a fast coarsening process, with dynamical scaling being obeyed for a restricted time regime. Below the gelation temperature, nearly the entire phase separation process is influenced by the gelling tendency of the gelatin. The rate of gelation relative to that of the phase separation determines the final morphology of the gel. A variety of morphologies are observed. Apart from slowing the separation, gelation is found to preclude the coarsening, which is dominated by hydrodynamics, and to cause dynamic scaling to fail as a consequence of the introduction of a wide range of distance scales. In this system, the effect of cross-link formation as a separation-enhancing force can be observed.

1. Introduction

In recent years the kinetics of phase separation in polymer mixtures has been widely studied, not least because of practical considerations: for example, phase separation kinetics determine the morphology of composite polymer materials[1] and the texture of processed food[2] and can play an important role in the optimizing of membrane properties.[3] Previous work has largely focused on pairs of synthetic polymers far from the glass transition.[4,5] Such blends are quenched from the homogeneous phase into a two-phase coexistence region by a rapid temperature step. The development and growth of inhomogeneities can be followed by monitoring the changes in a scattering pattern after the quench. Under favorable circumstances, for the case of quenches into the unstable region of the phase diagram, the interdiffusion of the separating polymers and the correlation length of the compositional fluctuations can be determined from the evolution of the peak in the scattering curve using the analysis due to Cahn and Hilliard.[6] In later stages of phase separation a power law behavior of the time dependence of the position and intensity of the maximum in the scattering pattern has been observed,[7,8] together with dynamic scaling; i.e., only one time-dependent length scale determines the evolution of the morphology.

A more complex situation is possible when one has a ternary polymer system of a polymer A, polymer B, and a solvent.[9–11] However, features qualitatively similar to those in binary mixtures are found, particularly in the situation when the solvent is an equally good solvent for both polymers—the so-called quasi-binary case.

In this report an account will be given of the phase separation kinetics of aqueous solutions of the biopolymers gelatin and dextran. Closely related gelatin/polysaccharide systems have important applications in the food and photographic industries. Of more fundamental interest is the fact that the system gelatin/dextran/water allows one to study the influence of gelation on the phase separation kinetics. Aqueous solutions containing gelatin and dextran, which on their own are both readily soluble in water, tend to separate to a gelatin-rich phase and a dextran-rich phase below a certain temperature. This gives rise to turbidity which eventually develops into two transparent layers. Deep quenches on systems with a high gelatin concentration form a macroscopic gel and do not show macroscopic phase separation.

In the context of phase separation, the existence of a gel point has a number of consequences. First, there is a large effect on the mobility of one or both of the components of the mixture which might be expected to be analogous to the effects of a glass transition in one of the components and would severely slow down the phase separation process. Second, gelation will lead to changes in the thermodynamics of mixing. As gelation proceeds, both the effective molecular mass of the gelatin and the width of the molecular mass distribution will increase. Thus the entropy of mixing will decrease and in effect the quench will become deeper with time. In addition, there will be an effect of the network elasticity on the free energy of mixing: gels with a low elasticity can be expected to tolerate only a limited degree of phase separation from a second polymer species. The time at which the elasticity effect becomes significant will depend on the relative rates of the gelation and phase separation. These differences can be expected to cause a considerable increase in complexity of phase separation behavior for these gelling systems over comparable simple polymer mixtures.

In the system gelatin/dextran/water, the phase separation temperature and the gelation temperature are dependent on the polymer composition, the total polymer concentration, and the amount of added salt (which alters the solvent quality). By varying these conditions, it is possible to control the interplay between gelation and separation, allowing initiation of the phase separation at temperatures either above or below the temperature at which gelation eventually takes place. In the latter case, one can tune the relative rates of phase separation and gelation. To anticipate the results, the interplay between phase separation and gelation determines both the final morphology of the macroscopic gel and the kinetics by which this morphology is achieved.

® Abstract published in *Advance ACS Abstracts,* May 1, 1995.

0024-9297/95/2228-4129$09.00/0

This interplay is complex and each process may have an effect on the other. For example, a nonequilibrium phase-separated morphology might be expected to be frozen by the onset of gelation, while, in contrast, the increase of the local gelatin concentration due to phase separation might cause gelation even when the average concentration is insufficient for gelation.

The large size of the inhomogeneities that usually develop after a quench into the coexistence region and the favorable refractive index mismatch between gelatin-rich and dextran-rich phases render small-angle light scattering an appropriate technique to study these phase separation kinetics. In particular, during later stages of the phase separation process, the time evolution is sufficiently slow to apply time-resolved elastic light scattering in which the scattering pattern is recorded at time intervals. Complementary real space data are obtained from light microscopy.

2. Theory of Phase Separation in Nongelling Mixtures

Fluctuations in concentration will tend to grow when a mixture is quenched into the unstable part of the phase diagram, as defined by the condition that the second derivative of the free energy, f, with respect to the concentration, c, $\partial^2 f/\partial c^2$, is negative. The boundary of this region is known as the spinodal curve. The well-known theory of Cahn and Hilliard[6,12] gives the result that one particular wavelength of fluctuations in the composition grows most rapidly, leading to a well-defined peak in the scattering pattern.

Briefly, the result is that the scattering intensity $I(q,t)$, which in an isotropic system can be expressed as

$$I(q,t) \propto \int \langle \delta c(\mathbf{r},t)\delta c(\mathbf{0},t)\rangle e^{i\mathbf{q}\mathbf{r}}\, d\mathbf{r} = \langle |\delta \tilde{c}(\mathbf{q},t)|^2 \rangle \quad (1)$$

where the absolute value q of the scattering vector $\mathbf{q}$ is defined as $(4\pi/\lambda)\sin(\theta/2)$ (λ is the wavelength and θ is the scattering angle), $\delta\tilde{c}(\mathbf{q},t)$ is the spatial Fourier transform of the fluctuations in the concentration $c(\mathbf{r},t)$, and the sharp brackets indicate an ensemble average, is given by

$$I(q,t) = I(q,0)e^{2R(q)t} \quad (2)$$

where we have neglected the effects of thermal fluctuations. The term $R(q)$, which describes the growth of fluctuations in time as a function of q, is known as the amplification factor and is given by

$$R(q) = -\Lambda(q)\left[\frac{\partial^2 f}{\partial c^2}q^2 + 2\kappa q^4\right] \quad (3)$$

$\Lambda(q)$ is the Onsager mobility coefficient, which might be q dependent, for instance in the case of hydrodynamic interactions.[13,14] κ is the constant of proportionality (>0) between the square of the linear concentration gradient and the associated free energy. $\partial^2 f/\partial c^2$ becomes negative below the spinodal (assuming an upper critical solution temperature) so for that case there will be a q range between zero and a critical value

$$q_c = \left[-\frac{\partial^2 f}{\partial c^2}\Big/2\kappa\right]^{1/2} \quad (4)$$

where $R(q)$ is positive ($\Lambda(q)$ is always positive). This will give rise to the buildup of phase-separated domains with sizes corresponding to these q values. When Λ is q-independent, $R(q)$ has a maximum at a q value given by

$$q_m = q_c/2^{1/2} \quad (5)$$

At q_m the concentration fluctuations grow faster than at all other q values. This is the origin of the "spinodal ring" in the two-dimensional scattering pattern of a phase-separating system. q_m will increase when the system is quenched deeper into the spinodal region. When Λ is q-dependent, q_c will stay the same, but q_m will be shifted.

The relation between q_m and the correlation length ξ of the concentration inhomogeneity is given by

$$q_m = 2\pi/\xi \quad (6)$$

The effective collective interdiffusion constant of the separating solutes is

$$D_{eff}(q) = -\frac{\Lambda(q)}{\partial^2 f/\partial c^2} \quad (7)$$

Now, $R(q)$ can be written as

$$R(q) = D_{eff}(q)q^2\left[1 - \frac{q^2}{2q_m^2}\right] \quad (8)$$

By plotting $R(q)/q^2$ against q^2 (Cahn–Hilliard plot), a straight line will result when D_{eff} is independent of q. From the slope and the intercept, D_{eff} and q_m can be calculated. Often, in order to be able to compare the coarsening of phase-separating systems at different temperatures and test for universal behavior, the processes are considered on a reduced time scale

$$\tau = (D_{eff}q_m^2)^{-1} \quad (9)$$

which is the time it takes to build up an inhomogeneity of the characteristic size $1/q_m$. τ is assumed to be the relevant unit of time for the description of the early-stage spinodal decomposition.

This linear theory predicts that the amplitude of a peak in the structure function should grow exponentially but the peak will remain at a fixed wave vector. However, nonlinear effects are important for all but the earliest times, and in practice the peak moves to smaller wave vectors in what is known as the intermediate stage. Ultimately, the compositions of the inhomogeneities are close to the equilibrium coexistence values and there is a pattern of domains separated by what are in effect equilibrium interfaces. In this late stage only one length scale, the mean domain size, is important, and thus we expect dynamic scaling to hold.[15] The scattering intensity takes the form

$$I(q,t) \propto q_m(t)^{-3}F[q/q_m(t)] \quad (10)$$

where $q_m(t)$ is the time-dependent reciprocal characteristic length of the coarsening system. All time dependence in the function $F(x)$ should be due to $q_m(t)$, implying that the shape of $I(q,t)$ is time-independent and that only one time scale is evolving as the phase separation proceeds. Dynamic scaling can be identified by assessing the validity of the relation

$$\frac{q_m(t)^3 I_m(t)}{s_2(t)} = \text{constant} \tag{11}$$

where $I_m(t)$ is the measured maximum in the scattering pattern and can be expressed, when dynamic scaling applies, by

$$I_m(t) \propto q_m(t)^{-3}\langle \delta n(t)^2\rangle F(1) \tag{12}$$

and $s_2(t)$ is given by

$$s_2(t) = \int_{q \ll q_m}^{q \gg q_m} I(q,t) q^2 \, dq \propto \langle \delta n(t)^2\rangle V \tag{13}$$

$I(q,t)$ is the intensity of the scattered light, $\langle \delta n(t)^2\rangle$ is the average square of the refractive index difference between the phases, V is the irradiated sample volume, and the constant of proportionality is time-independent. $s_2(t)$ can be evaluated when experimental data are available at all q values where $I(q,t)$ is significantly different from zero.

The growth of the characteristic domain size $q_m(t)$ often follows a power law in the late stage; the exponent depends on the dominant mechanism for mass transport. For diffusive growth one expects an exponent of $-1/3$ from the Lifshitz–Slyozov law,[16] whereas for growth dominated by hydrodynamic flows one expects an exponent of -1.[17] In reality, the relative importance of these two mechanisms may change with time through the late stage, leading to different apparent exponents during a long crossover stage.

In this late stage of phase separation the existence of sharp interfaces between the domains implies that the asymptotic behavior at high q is given by Porod's law:[18]

$$I_{asympt}(q,t) \propto \langle \delta n(t)^2\rangle \frac{A(t)}{q^4} \tag{14}$$

where $A(t)$ is the area of the interface between phase domains in the irradiated volume. Porod's law is valid if all distance scales for which there are inhomogeneities of refractive index are much larger than $1/q$. Combining eqs 13 and 14 leads to

$$\ln\left(\frac{I_{asympt}(q,t)}{s_2(q,t)}\right) = \ln\left(\frac{A(t)}{V}\right) - 4\ln(q) \tag{15}$$

which shows that from a full knowledge of $I(q,t)$, the time-dependent scattering interface can be obtained.

3. Experimental Section

Samples. Dextran and porcine skin gelatin were purchased from Sigma Chemical Co. The weight-average molecular mass of dextran was 1.6×10^5 g mol^{-1}, determined by wide-angle light scattering. The bloom number of the gelatin reported by the manufacturer was 175; this corresponds roughly to a weight-average molecular mass of 2.5×10^5 g mol^{-1}.[19] From these values of the molecular masses, it can be estimated that the radii of gyration are smaller than 0.1 μm, which is an order of magnitude smaller than the inhomogeneities observed in the phase-separating systems. An aqueous solution of 0.5 m NaCl was used as solvent. The gelatin and dextran were used without further purification.

The compositional phase diagram shown schematically in Figure 1 was determined by leaving sealed samples for several days in a temperature-controlled water bath. Turbid solutions were considered to be phase separated. Addition of salt to the water provides a phase transition temperature for a convenient range of compositions between the gelation temperature and 100 °C, which is desirable from an experimental point of view. A sample was described as gelled when turning the sample bottle did not result in a flowing liquid with a smooth surface. At 18 °C, the gel line and the coexistence line divide the compositional phase diagram into four regions: fluid/clear, fluid/turbid, gelled/clear, and gelled/turbid. On increasing the temperature, the coexistence line moves to higher total polymer concentrations while the gel line shifts to higher gelatin concentrations. Roughly speaking, for total polymer concentrations between 4 and 10% (w/w), phase transitions with temperature between the gel temperatures and boiling point can be found. Above 25 °C the gel line moves out of the investigated part of the phase diagram. Microscope images of fluid/turbid samples at room temperature showed clustered spheres of gelled gelatin-rich phase dispersed in the fluid dextran-rich phase. The size and clustering properties of the gelatin spheres will be the subject of a future publication.

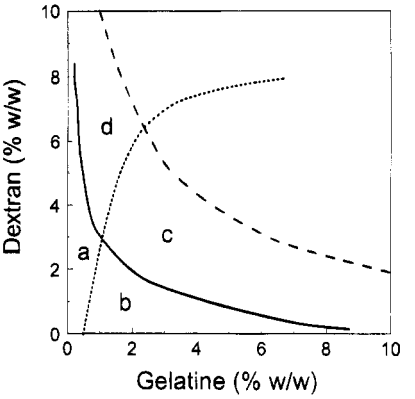

Figure 1. Compositional phase diagram (schematic) of a solution of gelatin and dextran in aqueous 0.5 m NaCl. Full line, coexistence line at 18 °C; dotted line, gel line at 18 °C; dashed line, coexistence line at 60 °C; a, clear fluid; b, clear gel; c, turbid gel; d, turbid fluid (metastable), all at 18 °C. Above 25 °C, the gel line is shifted to gelatin concentrations higher than 10%.

As no tie lines were determined, the critical line is not accurately known. Measurement of the two volumes after complete separation, which should be nearly equal close to the critical temperature and composition, indicates that the critical line is between gelatin/dextran weight ratios of 1:1 and 3:2. The composition of the solution used in this work was 4.2% gelatin and 4.2% dextran (w/w) in 0.5 m NaCl, which is therefore close to critical. The phase transition temperature of this solution is 38 °C and the gelation temperature 25 °C. A typical difference in refractive index between separated domains of dextran and gelatin (Δn) is 0.006 (the difference between 10% dextran and 10% gelatin). Considering that the wavelength (λ) is 0.6328 μm and the size of the inhomogeneities does not exceed 30 μm, it appears that the condition for Rayleigh–Gans scattering of $\lambda/\Delta n$ being much less than the size is met.

Instrumentation. The light scattering apparatus is shown schematically in Figure 2. A He–Ne laser beam (wavelength 0.6328 μm) passes through a pinhole of 100 μm diameter to enhance the beam homogeneity. The light from the zero-order maximum of the pinhole is expanded and converted into a parallel beam with the lens L1. After the diaphragm D, the beam has a diameter of about 1 mm. The mirror M deflects the beam to a vertical direction through the sample mounted on a heating/cooling stage (Linkam TMS600). The aperture of the stage is 2.5 mm. The transmitted beam is focused by lens L2 (diameter 100 mm, focal length 150 mm) onto the beam stop (BS) of diameter 5 mm. The lens L2 also brings the scattered light as a slightly convergent beam toward the detector, an OMA Vision-CCD camera (EG&G) fitted with a Peltier cooled charge coupled device (CCD) as an efficient, low noise photon detector. The light-sensitive array size is 10 × 10 mm, divided in 512 × 512 cells. Lens L2 is positioned to catch all light scattered at angles up to 15°. The scattered

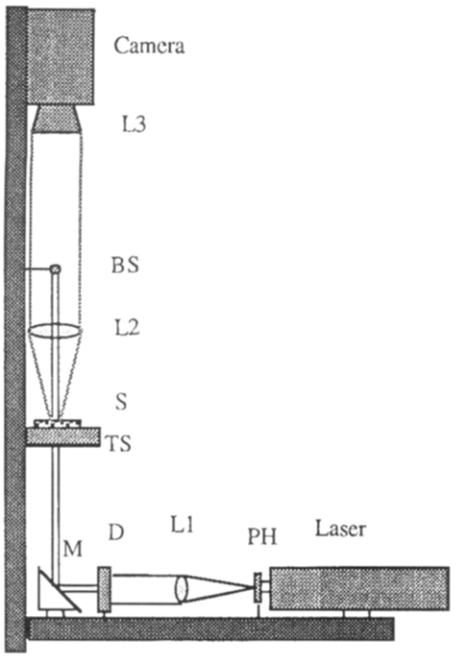

Figure 2. Diagram of the small-angle static light scattering instrument. PH, pinhole; L1 and L2, biconvex lenses; D, diaphragm; M, mirror; TS, heating/cooling stage; S, sample; BS, beam stop; L3, camera lens.

beam reaches the CCD array by way of a standard camera lens (L3) which is focused on the plane of the beam stop. The diameter of the part of the CCD device illuminated by scattered light is about 5 mm. Effectively, the scattering pattern is recorded as if it were in a plane about 12 mm above the sample. This is well into the "far field" if we consider that the sizes of the structures that were observed were less than 0.03 mm. In this configuration the angular range over which reliable data can be collected is 0.5−13°, corresponding to $0.1 < q/\mu m^{-1} < 2.3$. The resolution in q is about 6%. The data from the camera were recorded on a personal computer as a two-dimensional array of intensity against position. These data sets were transferred to DEC workstations for further detailed analysis. From the reproducibility of pinhole images, it was concluded that instability of the laser intensity did not have to be taken into account. Therefore no beam monitor was used.

Light microscope images were obtained with a Zeiss Axioplan microscope in the phase contrast mode. The same heating/cooling stage, temperature controller, and sample container were used as for the light scattering experiments.

Calibration. The fringe pattern from a pinhole of 30 μm diameter placed at the sample position was measured as a calibration sample and to test whether the image recorded on the camera can be treated as a far-field scattering pattern of the inhomogeneities in the sample. The scattering pattern or the differential cross section of a pinhole, defined as the fraction of the incident photons diffracted per unit solid angle $d\Omega$ at an angle θ with the incident beam, is given by

$$\left(\frac{d\sigma}{d\Omega}\right)_p = A_p\left[2\frac{J_1(kR\sin(\theta))}{kR\sin(\theta)}\right]^2 \tag{16}$$

where A_p is the area of the pinhole, J_1 is the first-order modified Bessel function, R is the radius of the pinhole, and k is equal to $2\pi/\lambda$ (λ is the wavelength). The angular calibration was obtained from the positions of the fringes of the diffraction pattern of the pinhole. On Fourier transforming the data, a satisfactory real space image of the pinhole was recovered, which confirmed that a far-field diffraction pattern was recorded on the camera.

The differential cross-section of the sample, $(d\sigma/d\Omega)_s$ in units of scattering cross-section per unit volume, was derived from the measured intensities of the fringes. When $I_p(\theta)$ and $I_s(\theta)$ are the measured intensities from the pinhole and the sample, respectively,

$$\left(\frac{d\sigma}{d\Omega}\right)_s = \left(\frac{d\sigma}{d\Omega}\right)_p \frac{I_s(\theta)}{I_p(\theta)}\frac{1}{DA_s} \tag{17}$$

where A_s is the illuminated area of the sample and D is the thickness of the sample.

In practice, because of a small background intensity, it was convenient to use the differences of intensity between consecutive maxima in the pinhole diffraction pattern. The ratios of these values with those calculated from the theoretical curve (eq 16) were used as a calibration curve for an absolute intensity scale. For a 30 μm pinhole, 10 fringes could be observed. This gave 11 maxima as points on a q calibration curve and 10 points on the intensity calibration curve. Second-order polynomials were fitted to these data sets and correction values evaluated for the 64 center positions of the radially averaged data bins. In actual experiments, before applying eq 17 to correct the measured intensity, a subtraction of background was made as discussed below.

Sample Environment and Data Collection. The sample container was a sapphire crucible with a depth of 1 mm. The hot, homogeneous sample solution was pipetted into the crucible, which was preheated on the heating/cooling stage to a temperature well above the phase transition temperature. The crucible was closed with a microscope cover slip. Prior to a quench, the sample temperature was equilibrated at about 45 °C for 20 min.

Quenches were performed from 45 °C to temperatures between 21 and 30 °C. The cooling rate of the stage was 90 °C/min. Measurements with a calibrated thermistor in the sample crucible showed that a homogeneous sample temperature was not achieved until at least 20 s after the destination temperature of the quench as indicated by the temperature controller was reached. Samples were selected for study that showed phase separation rates well below these cooling rates. After the quench the scattering pattern was recorded at a series of times. The time needed to register the scattering pattern is 2.5 s. The amount of multiple scattering was estimated by following the intensity of the transmitted beam during some of the phase separations. This intensity is never reduced by more than 10%, which allows the effects of multiple scattering to be ignored.

The peak in the scattering known as the spinodal ring that appears some time after the quench was isotropic and could be used to determine the center of the scattering pattern. This center was used in the calculation of the radial averages of the data. In calculating the radial average, the intensities of all pixels that have a certain distance from the center are added and divided by the number of such pixels. Reflections of the transmitted beam from the lens L2 and the sample could not be entirely avoided. For these reasons some areas had to be excluded from the radial averages of the two-dimensional data. The area around the beam stop and its support post was similarly excluded from the radial average.

Data Analysis. Background scattering had to be eliminated before the radially averaged counts from the camera were put on a scale of q and absolute intensity. If the background is defined as the intensity that is not due to phase separation, there are four contributing factors: (i) dark noise from the camera, (ii) dust in the sample and scratches on the sapphire crucible and cover slide, which are particularly significant at the lowest q values, (iii) scattering due to fluctuations in the overall polymer concentration, and (iv) an incoherent contribution. The contributions from (i) and (ii) were found to be the most important. To deal with this background, the scattering pattern collected about 30 s after the destination temperature of the quench was reached but before any significant increase in scattered intensity was observed was subtracted from all the subsequent scattering patterns.

4. Results and Discussion

General Phenomenology. In this section we discuss the results of quenching solutions with a composi-

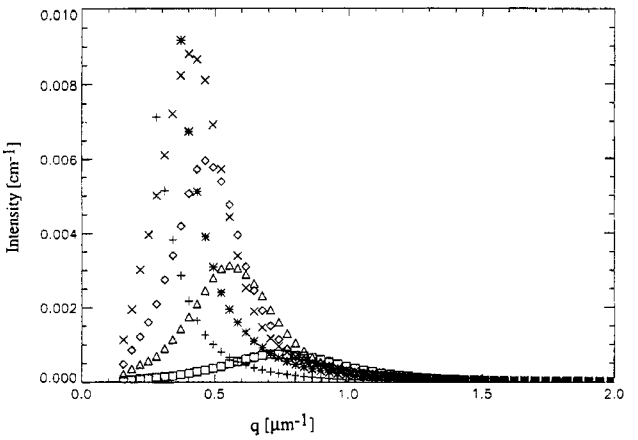

Figure 3. Light scattering pattern after a quench to 30 °C of 4.2% dextran/4.2% gelatin solution (phase transition at 38 °C, gelation temperature 25 °C): (□) 314 s; (△) 470 s; (◇) 628 s; (×) 786 s; (*) 1268 s; (+) 4018 s.

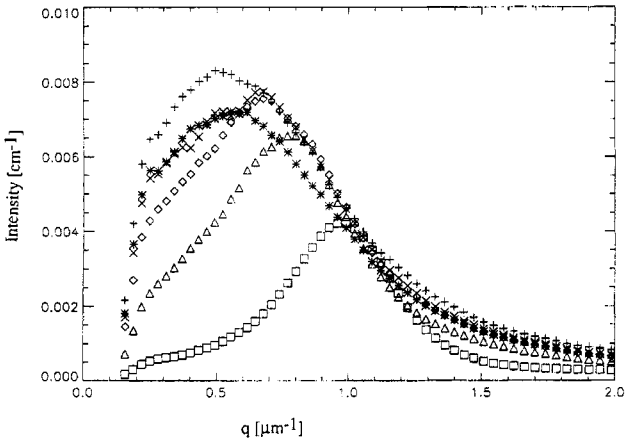

Figure 4. Light scattering pattern after a quench to 21 °C for 4.2% dextran/4.2% gelatin solution: (□) 126 s; (△) 378 s; (◇) 560 s; (×) 744 s; (*) 1160 s; (+) 1382 s.

tion of 4.2%/4.2%/91.6% gelatin/dextran/0.5 *m* aqueous NaCl into the two-phase region of the phase diagram. After discussing the general phenomena that occur for all final temperatures used, we will then treat the difference in behavior that is observed when the final quench temperature is above or below the gelation temperature, which is marked by a transition from a fluid to a weak, non-self-supporting gel, and a sudden increase in the loss and storage moduli.

In all cases after a quench into the two-phase region of the phase diagram the scattering pattern shows a ring in the two-dimensional scattering pattern, corresponding to a peak in radially averaged scattered intensity. For example, Figure 3 shows the development with time of the radially averaged scattering intensity after a quench to 30 °C (below the phase separation temperature but above the gelation temperature), while Figure 4 is the corresponding plot for a quench to 21 °C (4 °C below the gelation temperature). The appearance of a broad peak is characteristic of spinodal decomposition. In each case, as time progresses the position of the peak moves to lower q and its intensity increases. This indicates that at least for q values in the range of q_m and higher we are outside the range of validity of the linear theory of spinodal decomposition; the morphology is coarsening.

There are both quantitative and qualitative differences between the behavior following quenches to 30 and 21 °C. At first, the position of the maximum is at a higher value of q for 21 °C than for 30 °C. This difference can be understood in terms of the linear theory; at the lower temperature $\partial^2 f/\partial c^2$ is more negative (eqs 5 and 6) and consequently the q-vector of the fastest growing composition fluctuation is larger. More interesting is the qualitatively different time evolution of the shapes of the curves at the two temperatures. Although in both cases the peak intensity increases and the position moves to lower q values, there is, in the low-temperature quench, a continuing growth of intensity at high q values, in contrast to the high-temperature quench. In addition, in the gelling system the rate of coarsening slows down, while at a similar stage of coarsening in the fluid system growth is still unrestricted.

Direct microscopic observation of the phase-separating systems shows a picture consistent with our scattering data. Phase contrast micrographs of the separating system at the two temperatures are shown in Figure 5. Initially, the pattern has the same, reticular, character for both 30 and 21 °C, consistent with a common mechanism of phase separation in the early stages. Qualitative differences appear at later times; at 30 °C droplet-like domains appear after about 10 min, a transition which does not take place for the quench to 21 °C. Subsequently, phase separation at 30 °C proceeds by the formation of large gelatin-rich spheres that grow by coalescence, whereas for the quench to 21 °C after about 20 min the morphology freezes when it is still reticular.

Comparison with Cahn–Hilliard Theory. Before discussing the differences in phase separation behavior that show up at later times, we first discuss the extent to which the phase separation behavior at early times can be accounted for by the classical, linearized theory of spinodal decomposition due to Cahn and Hilliard. For the samples quenched to 30 °C, the logarithm of the scattered intensity $\ln[I(q,t)]$ plotted versus time (Figure 6) does show an initial linear increase, as predicted by eq 2. At temperatures below 27 °C, however, any initial linear growth regime is of very short duration, making it hard to observe. The linear growth at 30 °C is followed by a well-defined crossover into a regime of slower time dependence. From this initial linearity we can conclude that the influence on the phase separation process of thermal noise can be neglected;[20] thus we should be able to test the validity of eq 3 by extracting the linear growth rates $R(q)$ from the straight lines and plotting $R(q)/q^2$ against q^2; if the mobility Λ is not dependent on q, this should yield a straight line (such plots are often known as Cahn–Hilliard plots). In fact, for our data the result of such a plot is very far from linear; Figure 7 shows a representative case. Similar behavior is observed at other temperatures. We even see a significant peak at a value of q^2 of 0.3 μm^{-2}, which in principle points at enhanced growth at that q value. At present it is not clear how to interpret this feature. A possible explanation of the overall curvature of the plot, due to Binder et al.,[21] is that there is more than one time scale governing the phase separation kinetics. The presence of slowly relaxing degrees of freedom is usually associated with glassy systems,[22] but it is conceivable that in our system some degree of freedom is brought out of equilibrium by the quench and relaxes in a nondiffusive way. A possible candidate is the conformational change of the gelatin chains at the onset of gel formation. However, there are other examples of Cahn–Hilliard plots of a phase-separating polymer

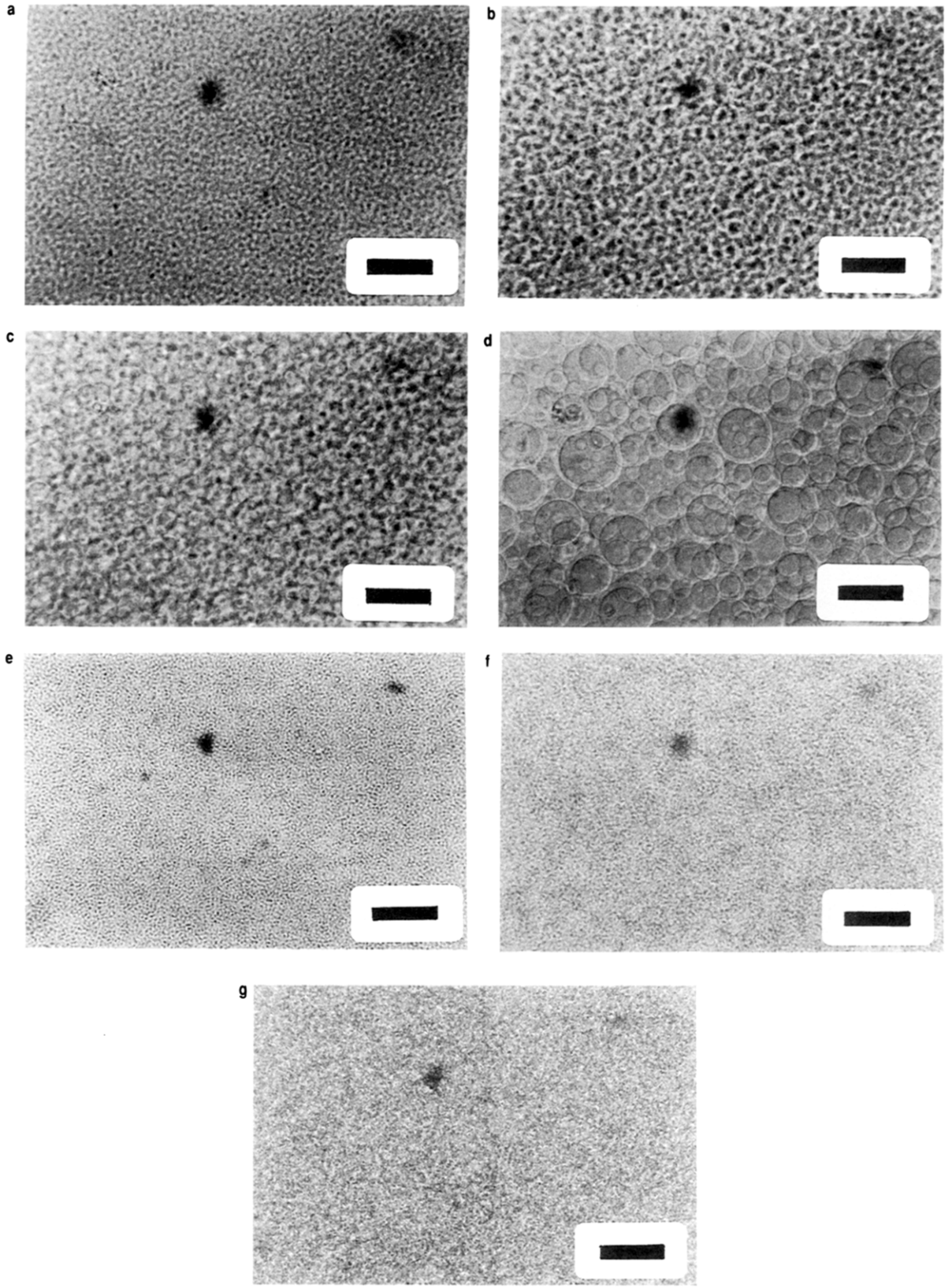

Figure 5. Phase contrast microscope images of the phase-separating gelatin/dextran solution at 30 (a–d) and 21 °C (e–g) at several times after the quench: (a) 240 s; (b) 600 s, (c) 780 s; (d) 1800 s; (e) 60 s; (f) 840 s; (g) 1440 s. The scale bar indicates 100 μm.

solution at a temperature far from the glass transition showing a comparable curvature,[10] so it may be that a nonlinear Cahn–Hilliard plot is a more general characteristic of polymer solutions. In that case hydrodynamic interactions, and the consequent q-dependent Onsager coefficients, would be the most probable source of the nonlinearity.

The utility of Cahn–Hilliard plots is that when they are linear, extrapolation to zero q allows one to extract the collective diffusion constant of the separating polymers. Thus one can obtain the parameters needed for calculating the reduced time scale by which phase separation processes at different temperatures can be compared. According to Binder et al.[21] this extrapola-

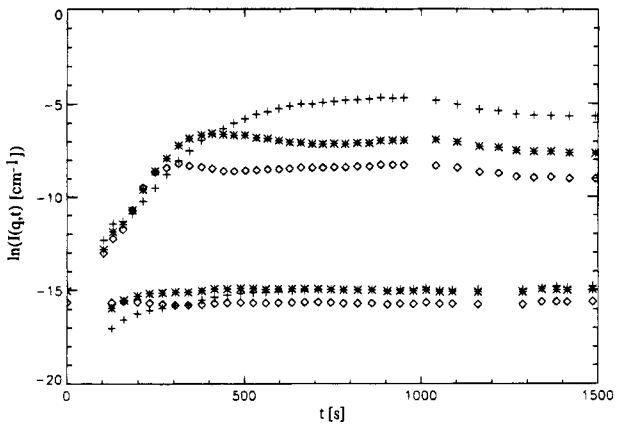

Figure 6. Growth of the scattering intensity at 30 (upper set) and 21 °C (lower set): (+) $q = 0.46\ \mu m^{-1}$; (*) $q = 0.77\ \mu m^{-1}$, (◇) $q = 1.09\ \mu m^{-1}$. The lower set has been shifted downward by 10 units.

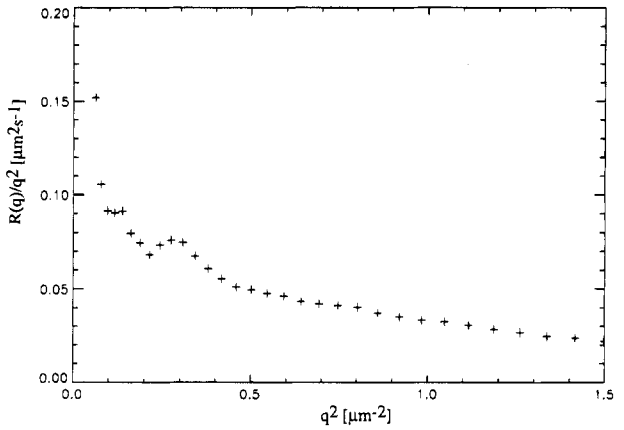

Figure 7. $R(q)/q^2$ versus q^2 at 30 °C. $R(q)$ is the initial linear growth rate.

tion is still valid even in the presence of slow modes. However, in practice, the quality of our data does not allow us to make this extrapolation. As a consequence, all our subsequent results are available only on an absolute time scale.

Moving beyond the early stages of phase separation, the most obvious feature is the coarsening of the phase-separated structure, manifested in the movement of the maximum in the scattering pattern to lower values of q. The position (q_m) and the intensity (I_m) of this maximum can be determined accurately up to a time at which the maximum has moved to such low angles that it becomes impossible to observe in the present setup; this time is about 2000 s for the quench to 30 °C.

Figure 8 shows the time dependence of q_m, the position of the maximum in the scattering intensity $I(q,t)$, for temperatures above and below the gelation temperature. At 30 °C, we do not see uniform power law behavior. Over the time range where a maximum in $I(q,t)$ could be measured, $q_m(t)$ decreases with time with a power varying between −0.6 and −1.2. This is a faster rate of coarsening than would be expected if diffusion provided the only transport mechanism, in which case one expects a power of −1/3; thus it appears that hydrodynamic mechanisms of transport play some role at these early times. The general behavior is in reasonable agreement with the power of −1 which is expected for the coarsening by rearrangement and coalescence of neighboring domains governed by hydrodynamics.[18] At about 700 s, the decrease of q_m becomes more rapid. The time at which this happens coincides

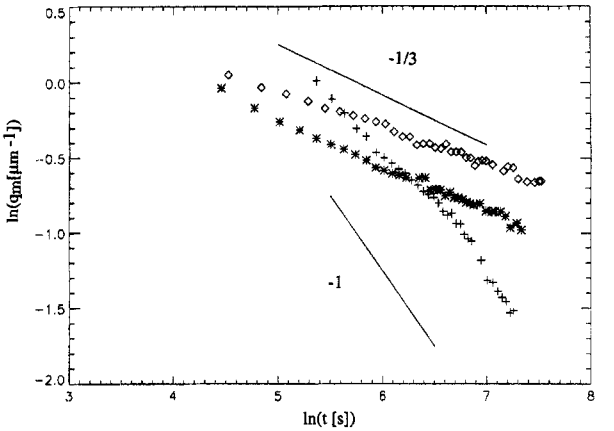

Figure 8. Time dependence of the position q_m of the scattering maximum: (+) 30 °C; (*) 25 °C; (◇) 21 °C.

with the time at which optical micrographs show a breakup of the gelatin phase into the isolated domains, seen in Figure 5; this suggests that a change in coarsening mechanism occurs when there is a qualitative change in morphology.

Recently, in the phase-separating system polystyrene/cyclohexane,[23] $q_m(t)$ was also found to decrease faster than by $t^{-1/3}$ from the earliest times after the quench, suggesting a contribution from hydrodynamics in the coarsening process. In that case, however, the coarsening slowed down with increasing time, approximating a $t^{-0.4}$ behavior, in contrast to the behavior of gelatin/dextran separation above the gelation temperature. In a single polymer/solvent system coarsening is expected to slow down due to the strong concentration dependence of the diffusion coefficient. Indeed in some cases coarsening may be completely arrested by the vitrification of the polymer-rich phase. However, in the gelatin/dextran system above the gelation temperature such effects are likely to be much weaker, as the changes in the overall polymer content of each phase, and thus their viscosity, during the phase separation process are likely to be relatively small.

We now turn to the coarsening behavior of the system quenched to below the gelation temperature, which proceeds in a manner rather different from the system quenched to 30 °C. Figure 8 shows that for a quench to 25 °C $q_m(t)$ follows a power law with an exponent close to 0.3 over the whole range of times for which a maximum in $I(q,t)$ was observed; there is no evidence for a change to a faster coarsening mechanism of the kind observed for the system above the gelation temperature. At 21 °C q_m decreases more slowly than by $t^{-0.3}$, most probably in anticipation of complete pinning down of the morphology by gelation.[24] For the system above the gelation temperature we associated a change in coarsening mechanism with a change in morphology; for the system below the gelation temperature the micrographs (Figure 5) show no qualitative changes in morphology, so we expect no change in coarsening mechanism. The power of 0.3 suggests that the domain growth is dominated by diffusion of solute with hydrodynamic flow playing little or no role. Our interpretation is that hydrodynamic flows, which at 30 °C allow fast coarsening by reshaping and coalescence of domains, are completely suppressed by the cross-linking of gelatin.

Finally, we turn our attention to the detailed form of the scattering function $I(q,t)$. First we will consider the case of the quench above the gelation temperature. A

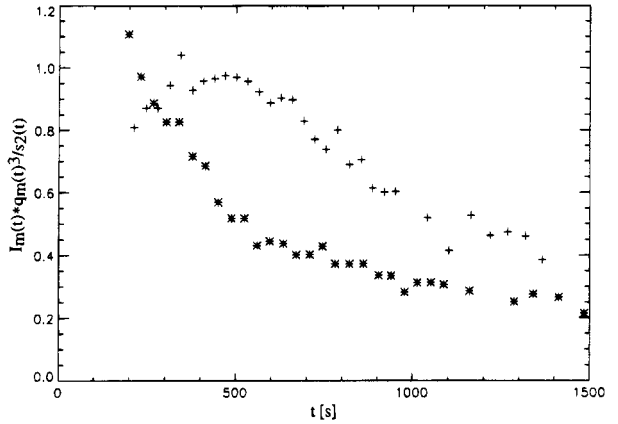

Figure 9. Test of the validity of dynamic scaling. Reduced amplitude $I_m(t)q_m(t)^3/\int I(q,t)q^2\,dq$ (eq 11) of the scattering maximum as a function of time above the gelation temperature ((+) 30 °C) and below ((*) 21 °C).

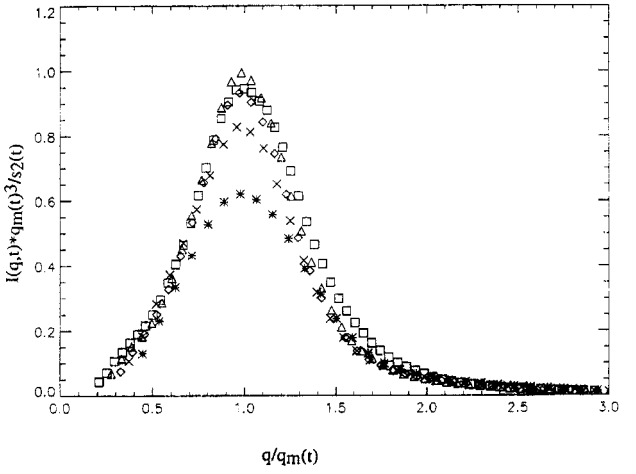

Figure 10. Dynamic scaling of scattering curves above the gelation temperature of gelatin. $I(q,t)q_m(t)^3/\int I(q,t)q^2\,dq$ vs q: (□) 314 s; (△) 470 s; (◇) 628 s; (×) 786 s; (*) 1268 s.

plot of the product $I_m(t)q_m(t)^3/\int I(q,t)q^2\,dq$ against time is shown in Figure 9 as a test of the validity of dynamic scaling (eq 11) for the phase separation both below and above the gelation temperature. For the quench at 30 °C this product is roughly constant up to about 600 s, indicating that dynamic scaling does hold. This can also be seen in Figure 10 which shows the scaled structure factor at various times. The data collapse onto a single curve up to 660 s when a qualitative change in the shape of the curve is observed. To our knowledge, no other detailed scaling analysis has been carried out for the case of phase separation in ternary polymer solutions. It is not possible to say whether this scaling behavior is a general feature of phase separation in polymer solutions. However, the change in morphology at about 700 s, as observed in Figure 5, coincides with the change in scaling behavior. After the crossover, the system is a fluid dextran-rich matrix with isolated gelatin-rich spheres. It is at first sight puzzling that the system should apparently have attained the late-stage scaling regime and then subsequently undergo a morphological transition with a consequent breakdown in scaling. This indicates that the phase volumes must still be changing slowly, despite the achievement of sharp phase boundaries. An explanation may lie in the polydispersity of the system; fast separation of the chemically different species may be followed by a much slower ageing process of partitioning of the molecular weight components of each chemical species.[25]

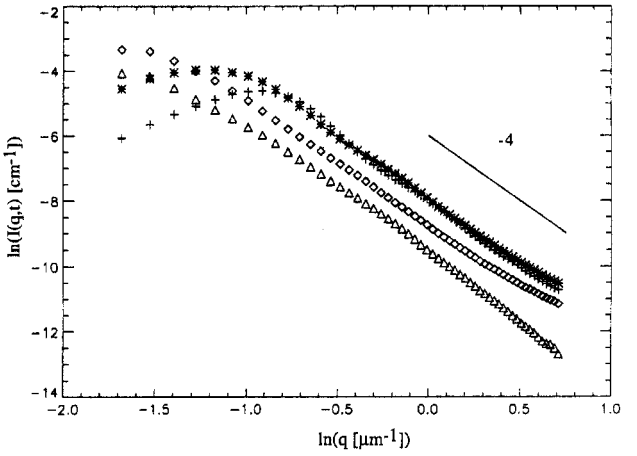

Figure 11. Late-stage power law behavior of the scattering intensity as a function of q at 30 °C: (+) 810 s; (*) 1042 s; (◇) 1918 s; (△) 5146 s.

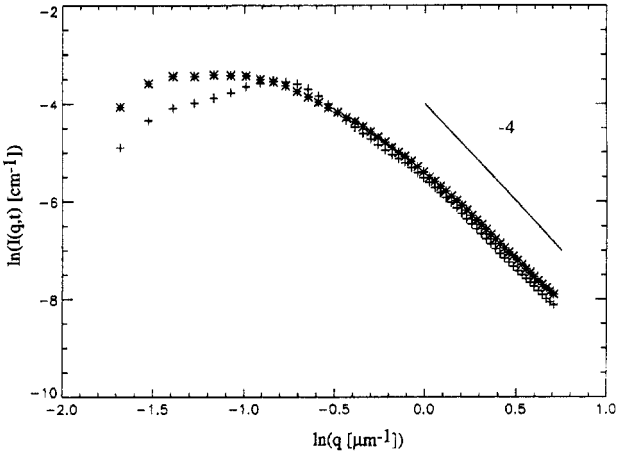

Figure 12. Late-stage power law behavior of the scattering intensity as a function of q at 25 °C: (+) 1030 s; (*) 4808 s.

Let us focus now on the shape of the curve at high q values which according to Porod's law should tell us something about the nature of the interfaces between the domains. This law (eq 14) predicts that a system consisting of domains separated by sharp interfaces will have $I(q,t)$ going as q^{-4} for large values of q. Figures 11 and 12 show that such behavior is observed both for quenches to 30 and 25 °C, respectively. The evolution of the high-q part of $I(q,t)$ can be followed for much longer times than the part that contains the maximum. The data shown have been collected during nearly 1.5 h after the quench. However, to apply eq 15 one has first to evaluate the integral of eq 13, for which values of $I(q,t)$ at all q values are required. For late stages at 30 °C, a considerable part of the scattering occurs at angles that are too small to be observed in the present setup. For this reason $\ln[I(q,t)]$ at 30 °C is plotted according to eq 14, i.e., not corrected for the time dependence of the difference in refractive index of the domains, whereas at 25 °C, for which nearly all scattered light can be collected during much longer times, data have been plotted according to eq 15. At 25 °C data at only two widely spaced times have been shown for the sake of clarity because of the slow rate of change.

At later times, the high-q part of the scattering pattern at 30 °C tends to a power law of q^{-4}. This suggests that sharp and smooth interfaces are being established between the gelatin-rich and dextran-rich regions. At the same time the intercept with the vertical axis of the linear part decreases with time and

the scattering maximum moves to lower q values. This intercept is proportional to the sum of the logarithms of the amount of scattering interface and the scattering strength $\langle \delta n(t)^2 \rangle$ (eq 15). $\langle \delta n(t)^2 \rangle$ can only remain constant or increase with time, so the observation of a decreasing intercept must be interpreted in terms of a decreasing amount of interface. A decreasing amount of interface together with the increase of domain size is consistent with coarsening by domain coalescence.

The high-q behavior in the gelling systems is quite different. At 21 °C (not shown), the Porod behavior turns out not to be reached in the q range available before the static gel stage is reached. At an intermediate temperature of 25 °C (Figure 12), the Porod behavior is reached, but the intercept, which in this case could be corrected for the time-dependent scattering strength $\langle \delta n(t)^2 \rangle$, does not decrease along with q_m as observed at 30 °C. After the Porod behavior has been established, it stays at the same level during the entire time of observation. These observations indicate that after gelation takes place the inhomogeneities at small distances are unchanging even when coarsening occurs at large distances.

This picture is consistent with the behavior of the shape of the whole scattering curve below the gelation temperature. At first, we note that at no time is dynamic scaling observed. This is qualitatively obvious from the shapes of the scattering curves shown in Figure 4, which continue to broaden up to the latest times, and is also apparent from Figure 9, which shows the product $I_m(q,t)q_m(t)^3/s_2(t)$ to be strongly time dependent from early times, indicating that dynamic scaling does not apply (eq 11). The apparent leveling of $I_m(t)q_m(t)^3/s_2(t)$ at later times is merely a reflection of the very slow rate at which the morphology changes.

The key differences that emerge from the shapes of the scattering curves for samples above and below the gelation temperature, then, are first that changes in morphology, reflected by alterations of the shape of the scattering curve, continue to take place while the total interfacial area, as revealed by Porod's law, remains the same. Secondly, we need to explain the introduction of a progressively wider range of length scales in the domain size distribution as time progresses in the sample quenched below the gelation temperature as compared to the sample quenched above the gelation temperature. To explain the first effect, we assume that the domains of gelled gelatin are still able to move and can thus form aggregates without coalescence. The cause of the growth of the characteristic distance scale is thus the clustering of gelled gelatin domains. The idea of clustering of gelatin domains is supported by observations made in phase-separated solutions containing much more dextran than gelatin.[26] In these systems, which at room temperature are basically suspensions of gelled spheres of gelatin in a dextran solution, the gelatin domains show a strong tendency to form clusters.

To explain the appearance on gelation of a wide range of length scales, it is natural to consider the effect of cross-linking for an explanation. When the gelatin starts to gel, the system changes from a mixed solution of linear polymers into a network of gelatin chains in a solution of dextran. Binder et al.[27] have developed a theory for the phase stability and separation kinetics of a linear polymer in a weakly cross-linked network of a different polymer which can account qualitatively for the observation made in the present system of a polymer, a network, and solvent. The effect on the free energy of mixing of a pair of polymers when one species is crosslinked is to replace the contribution from the translational entropy of this species by a term expressing the elastic energy of its network. The effect of gelation is to increase the spinodal temperature and consequently as gelation proceeds, the system moves deeper into the subspinodal region of the phase diagram of mixing. This increase with time of the effective quench depth will lead the range of unstable fluctuation wavelengths to extend to higher q values and will result in increased scattering at these q values. Conversely, the growth of intensity at low q values will be hindered by the effect of network elasticity; the growth of large dextran-rich domains would cause a distortion of the network, with a consequent elastic penalty. In the limit of extremely fast cross-linking compared to the rate of phase separation, this effect leads to microphase separation, as observed in semi-interpenetrating networks.[28] Of course, in our case, the rates of gelation and phase separation are comparable, and thus considerable further theoretical work will be necessary before any quantitative comparisons can be made.

Recently, excess high q scattering was also observed in the phase separation of the mixture gelatin/water/methanol.[24] In that case another explanation was proposed; the high q scattering was ascribed directly to the cross-links between gelatin chains. Our system is different in that the gelatin does not separate from the solvent but from a cosolute; thus the gelatin always remains in a good solvent environment. Aqueous solutions of gelatin in 0.5 m NaCl, either gelled or not, do not give rise to the strong high q scattering observed in partly phase-separated aqueous dextran/gelatin gels. Therefore the explanation of the scattering at high q in terms of concentration differences of dextran and gelatin therefore seems to be justified.

5. Conclusions

The evolution of the phase separation in a solution of dextran and gelatin after quenches into the biphasic region of the phase diagram above and below the gelation temperature of gelatin has been followed by static small-angle light scattering and phase contrast microscopy. In the early stages of phase separation, which are similar under both gelling and nongelling conditions, a peak appears in the scattering pattern as expected for a spinodal decomposition process. However, at no experimentally accessible time is the early, linear stage of spinodal decomposition observed. At later times the gelation starts to exert a considerable influence on the system morphology and the kinetics of the phase separation process. At temperatures where gelation occurs, the growth of the characteristic domain size closely follows a $t^{1/3}$ dependence. This suggests growth by a diffusion mechanism. Above the gelation temperature a growth varying between $t^{0.6}$ and $t^{1.2}$ is observed, which suggests that the coarsening process is affected and eventually dominated by hydrodynamics. The detailed growth behavior of the domains matches with both a failure of dynamic scaling of the structure function and a qualitative change in the morphology observed microscopically. The shape of the structure function of the inhomogeneities below and above the gelation temperature displays larger differences at longer times.

Gelation tends to slow the growth of the scattered intensity at low q (near and lower than the position of

the maximum) while causing an increase in scattering at high q when compared with nongelling solutions. This behavior, reflected in the failure of dynamic scaling and the absence of the usual q^{-4} Porod's power law dependence in the highest q range, is interpreted as the introduction by gelation of a range of distance scales smaller than the characteristic domain size. A tentative explanation is given in terms of the influence of cross-linking of gelatin on the phase diagram. It is suggested that, due to the cross-linking in the course of the phase separation, the system finds itself deeper in the spinodal region. This causes growth of concentration fluctuations of shorter wavelength. From the observation that below the gelation temperature the scattering peak associated with the characteristic domain size is still moving to lower q values whereas the amount of interface between the phases has become independent of time, it is concluded that gelled gelatin-rich regions retain sufficient freedom of motion to contribute to the coarsening of the morphology by aggregation without complete coalescence.

A quantitative treatment of the scattering behavior of a system that gels and phase separates at comparable rates is not possible at present due to the lack of a comprehensive theory. Such a theory would have to involve the strong coupling between the gelation and the phase separation processes. The system described in the present work is far from the ideal "chemically quenched" situation in which cross-linking is much faster than phase separation for which the theory of Binder and Frisch[27] was developed. The observed changes in the peak positions and intensities are probably a manifestation of this coupling. It suggests that the network which is formed can rearrange and continue to phase separate in a way which would not be possible were the gelation to be instantaneous. This will influence the morphology of the network in the final gel.

References and Notes

(1) E.g.: *Polymer Blends and Alloys*. Folkes, M. J., Hope, P. S., Eds.; Blackie Academic & Professional: London, 1993.
(2) Lewis, M. J. In *Physical Properties of Foods and Food Processing Systems*; Ellis Horwood Series in Food Science and Technology; Ellis Horwood: Chichester, England, 1987.
(3) Petrak, K. L. *J. Appl. Polym. Sci.* **1984**, *29*, 555.
(4) Snyder, H. L.; Meakin, P.; Reich, S. *Macromolecules* **1983**, *16*, 757.
(5) Nishi, T.; Wang, T. T.; Kwei, T. K. *Macromolecules* **1975**, *8*, 277.
(6) Cahn, J. W.; Hilliard, J. E. *J. Chem. Phys.* **1958**, *28*, 258.
(7) Hashimoto, T.; Itakura, M.; Shimidzu, N. *J. Chem. Phys.* **1986**, *85*, 6773.
(8) Izumitani, T.; Takenaka, M.; Hashimoto, T. *J. Chem. Phys.* **1989**, *92*, 3213.
(9) Hashimoto, T.; Sasaki, K.; Kawai, H. *Macromolecules* **1984**, *17*, 2812.
(10) Sasaki, K.; Hashimoto, T. *Macromolecules* **1984**, *17*, 2818.
(11) Kuwahara, N.; Kubota, K. *Phys. Rev. A* **1992**, *45*, 7385.
(12) Cahn, J. W. *J. Chem. Phys.* **1965**, *42*, 93.
(13) de Gennes, P.-G. *J. Chem. Phys.* **1980**, *72*, 4756.
(14) Binder, K. *J. Chem. Phys.* **1983**, *79*, 6387.
(15) Binder, K.; Stauffer, D. *Phys. Rev. Lett.* **1974**, *33*, 1006; *Adv. Phys.* **1976**, *25*, 343.
(16) Lifshitz, I. M.; Slyozov, V. V. *J. Phys. Chem. Solids* **1961**, *19*, 35.
(17) Siggia, E. D. *Phys. Rev. A* **1979**, *20*, 595.
(18) Glatter, O.; Kratky, O. *Small Angle X-ray Scattering*; Academic Press: New York, 1982.
(19) Data kindly provided by Sanofi Bio-Industries.
(20) Cook, H. E. *Acta Metall.* **1970**, *18*, 297.
(21) Binder, K.; Frisch, H. L.; Jäckle, J. *J. Chem. Phys.* **1986**, *85*, 1505.
(22) Andreev, N. S.; Bioko, G. G.; Bokov, N. A. *J. Non-Cryst. Solids* **1970**, *5*, 41.
(23) Lal, J.; Bansil, R. *Macromolecules* **1991**, *24*, 290.
(24) Bansil, R.; Lal, J.; Carvalho, J. L. *Polymer* **1992**, *33*, 2961.
(25) Koningsveld, R.; Solc, K.; MacKnight, W. J. *Macromolecules* **1993**, *26*, 6676.
(26) Tromp, R. H.; Rennie, A. R.; Jones, R. A. L., to be published.
(27) Binder, K.; Frisch, H. L. *J. Chem. Phys.* **1984**, *81*, 2126.
(28) Bauer, B. J.; Briber, R. M.; Han, C. C. *Macromolecules* **1989**, *22*, 940.

MA9461714